Influence of the Preparation Conditions on the Reaction Performance on Steam Reforming of Methanol in a Cu/Zn/Al model catalyst

Meng-qian Li, Sen Yao, Xing-yu Li, Fen-fen Du, Hao-ran Shi, Xu-bin Guan, Zhao-shun Zhang*

School of Chemistry and Chemical Engineering, Qufu Normal University, Qufu 273165, China

* Corresponding author. Tel.: +86 537 4456301;

E-mail: zzs@qfnu.edu.cn (Zhao-shun Zhang).

Abstract

The model Cu/Zn/Al catalysts with different calcination temperature were prepared by hydrothermal method. The catalysts were characterized by XRD, BET, SEM, CO_2-TPD, H_2-TPR, TG, CH_3OH-TPD and CO_2+H_2-TPSR. The effect of different calcination temperature on structure, stability and catalytic performance for methanol steam reforming at the conditions of 200-320℃ was also represented. The results of present study show that the different calcination temperature of Cu/Zn/Al catalysts had an obvious influence on the physical characteristics and catalytic performance of the methanol steam reforming.

1. Introduction

As an ideal liquid fuel, methanol has a wide variety of sources, lower price, easy to store and transport, and has higher energy density. Therefore, the methanol can be favoured transformed to hydrogen by catalytic reforming reaction at relatively low temperatures (200-300℃) [1-4]. At present, the mainly applied methods of hydrogen production from methanol contained partial oxidation of methanol (POM) and steam reforming of methanol (SRM) [5]. The considerable thermal was released during the POM process, leading to it was difficult to control the reaction temperatures, and the catalyst easy to sinter and produces less hydrogen. On the contrary, SRM has excellent efficiency during hydrogen producing, lower reaction temperatures and fewer CO formation. It is the preferred method of producing hydrogen from methanol on commercial scale [6, 7].

$CuO/ZnO/Al_2O_3$ catalysts were widely used in steam reforming of methanol [8, 9], because of its excellent performance during low temperature range and select hydrogen selectivity [3]. The mainly preparation methods for $CuO/ZnO/Al_2O_3$ catalysts were co-precipitation and hydrothermal methods. Commonly, it shows lower specific surface area for $CuO/ZnO/Al_2O_3$ catalysts prepared by co-precipitation, and poorly particle homogeneity. In contrast, the $CuO/ZnO/Al_2O_3$ catalysts, which prepared by the hydrothermal method, has uniform particles and larger surface area. It should be noted that the calcination temperature has a significant impact on the metal support interaction.

This paper prepared $CuO/ZnO/Al_2O_3$ catalysts by hydrothermal method, and urea was selected as the precipitating agent, PVP was introduced to improve the micro-morphology of catalysts. Moreover, the structure, reaction behaviours and mechanism in methanol steam reforming reaction were investigated by XRD, BET, SEM, CO_2-TPD, H_2-TPR, TG/DSC, CH_3OH-TPD, CO_2+H_2-TPSR for $CuO/ZnO/Al_2O_3$ catalysts.

2. Experimental

2.1 Catalyst preparation

Catalyst samples were prepared by hydrothermal method. All reagents used in this work were of analytical quality provided by Sinopharm Chemical Reagent Co., Ltd. All samples were prepared by the following method: 4.6 mmol $Cu(NO_3)_2·3H_2O$, 4.3 mmol $Zn(NO_3)_2·6H_2O$ and 1.1 mmol $Al(NO_3)_3·9H_2O$ were dissolved in 80 ml distilled water. Subsequently, 0.9696 g urea as the precipitant and 0.8880 g Polyvinylpyrrolidone (PVP) were added into the above mixture. After stirring, the mixture transferred to a 100 ml Teflon-lined autoclave. The

hydrothermal treatment was ducted at 180℃, using 2℃/min ramp, for 6 h. The autoclave was then cooled down to ambient temperature. The products were harvested by filtration, thoroughly washed three times using deionized water and ethanol, and then dried in an oven at 120℃. Finally, the samples were calcined at different given temperatures (400, 450 and 500℃) for 6 h. The prepared catalysts are named as CZA-X, in which X represents the calcination temperature, such as CZA-400, CZA-450, CZA-500.

2.2 Characterization

Powder X-ray diffraction (XRD) measurements were performed on a X'pert[3] X-ray diffractometer (PANalytical, Netherlands), using Cu Kα radiation, operating at 40kV and 30 mA in the range of 2θ=10° - 80°.

Brunauer-Emmett-Teller (BET) surface area and Barret-Joyner-Halenda (BJH) mesopore were measured by nitrogen adsorption-desorption on a Kubo-X1000 physisorption instrument (Beijing Builder Electronic Technology Co., Ltd, China) at -196℃ after the sample materials were degassed at 200℃ for 2h.

Scanning electron microscopy (SEM) images were obtained on a Sigma-500 scanning electron microscope (Carl Zeiss AG, Germany) to observe the morphology and microstructure of the catalysts pre-treated by sputtered.

The TG measurements were recorded by a STA449-F5 thermal analyser (NETZSCH, Germany). About 10 mg of the samples was put in a Pt-Rh crucible and positioned on the TG/DSC sample holder. An empty Pt-Rh crucible was used for the reference, obtaining the baseline according to the instrument manufacture's instruction. The materials were heated using a linear programming up to 800℃ by a heating rate of 10℃/min under flowing synthetic air atmosphere (70ml/min).

The temperature-programmed reduction of H_2 (H_2-TPR) was performed on an AMI-300 Chemisorption (Altamira Instruments, USA), using a 5 vol% H_2/Ar as reduction gas in a quartz micro-reactor. Typically, 50 mg of freshly calcined catalyst was placed on top of silica wool in the reactor pre-treated at 150℃ for 60 min under Ar (50 ml/min). After catalyst was cooled to room temperature, the flow rate of reducing atmosphere was kept at 50 ml/min and the temperature was elevated from ambient temperature to 600℃ at a rate of 10℃/min. The amount of hydrogen consumption was monitored by thermal conductivity detector (TCD). The alkali property of the sample was measured by CO_2-TPD and the exposed Cu surface area (S_{Cu}) in the reduced catalyst was measured by method of N_2O oxidation. Experiments were performed on the same apparatus as described above. For the CO_2-TPD experiment, 50 mg of samples were reduced at 300℃ in a flow of 5 vol% H_2/Ar (50ml/min) for 30 min and then cooled to 80℃ under He flow. The pre-treated samples were saturated with 20% CO_2/He (25 ml/min) at 80℃ for 30 min and then flushed with He flow. Finally, the CO_2-TPD experiments were conducted from 80℃ to 800℃ at a heating rate of 10℃/min under He flow (30 ml/min), and the desorbed CO_2 molecules were detected and recorded by thermal conductivity detector (TCD). For N_2O titration, use the same amount of catalyst as in CO_2-TPD. The samples were pre-treated at 400℃ for 60 min under 50 ml/min Ar flow. The sample was then cooled down to ambient temperature, the flow rate of 5 vol% H_2/Ar reducing atmosphere was kept at 50 ml/min and the temperature was elevated from ambient temperature to 400℃ at a rate of 10℃/min. The amount of hydrogen consumption in first TPR was denoted as A_1. Then, it was purged with Ar and cooled to 90℃. Surface copper atoms were oxidized in 50 ml/min 1% N_2O/N_2 at 90℃ for 30 min, and then flushed with Ar to remove the oxidant. Subsequently, the catalyst was cooled to room temperature to start another TPR run. Hydrogen consumption in the second TPR was denoted as A_2. The equations involved in the whole reaction are shown in 2.1-2.3:

$$CuO + H_2 = Cu + H_2O \qquad\qquad 2.1$$

$$2Cu + N_2O = Cu_2O + N_2 \qquad\qquad 2.2$$

$$Cu_2O + H_2 = 2Cu + H_2O \qquad\qquad 2.3$$
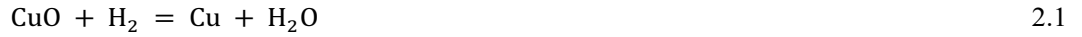
The dispersion of Cu (D_{Cu} %) and exposed Cu surface area (S_{Cu} m^2/g) were calculated as 2.4-2.5 [10]:

$$D_{Cu}(\%) = 2\frac{A_2}{A_1} \qquad\qquad 2.4$$

$$S_{Cu}(m^2/g) = 2\frac{A_2 N_A}{A_1 \times M_{Cu} \times 1.4 \times 10^{19}} \qquad\qquad 2.5$$

Where M_{Cu}=63.54 g/mol (relative atomic mass), N_A=6.02×10^23 mol^-1 (Avogadro constant), 1.4×10^19 is copper atom surface density per square meter.

The temperature-programmed desorption of CH_3OH (CH_3OH-TPD) and the CO_2+H_2 the temperature-programmed surface reaction (CO_2 + H_2-TPSR) was conducted on an AMI-300 instrument equipped with a Omnistar GSD-320 mass spectrometry (Pfeiffer, Germany) to monitor products. For the CH_3OH-TPD experiment, the catalysts (50 mg) were first pre-treated at 300°C for 30 min, after temperature was decrease to 100°C and then at the flow rate of 17 vol% CH_3OH/Ar (30 ml/min Ar through a bubbler containing methanol at 25°C) for 30min, to remove the physiosorbed CH_3OH, the catalyst bed was flush with Ar until the signal of mass spectrometry for CH_3OH was not changing any more. Finally, the catalyst was heated to 400°C at the rate of 10°C/min and maintained 15min. In CO_2 + H_2-TPSR experiments, the pre-treated catalyst is the same as that for CO_2-TPD. The catalyst was also adsorption of CO_2, after a Ar flushing for 30 min, the sample was heated to 400°C at 10% H_2/Ar atmosphere.

2.3 Evaluation of catalysts

The catalytic performance evaluation of the CZA-X for SRM was conducted in a quartz tube reactor under atmospheric pressure. 150 mg catalysts were first diluted with quartz sand and packed into the quartz tubular reactor and reaction at given temperatures (200, 240, 280, 320°C). Before each experiment the catalyst was pre-reduced in 10% H_2/N_2 flow (100 ml/min) at 300°C for 2h. The water to methanol mol ratio at feed stream was 2 into the carburettor, after vaporization, the mixture is carried to the reaction system via N_2 (53.33% H_2O /26.6% CH_3OH/N_2). Effluent gases were analysed on-line by a SP-6890 gas chromatograph (Lunan-Ruihong, China) equipped with a thermal conductivity detector, in which TDX-01 column (2m × 3 mm) was used to separate reaction products. The catalytic calculated based on CH_3OH consumption and CO_2/CO production, as 2.6-2.8 described below:

$$\chi_{CH_3OH} = \frac{Q_{CH_3OH_{input}} - Q_{CH_3OH_{output}}}{Q_{CH_3OH_{input}}} \qquad\qquad 2.6$$

$$S_{CO} = \frac{Y_{CO}}{\chi_{CH_3OH}} \qquad\qquad 2.7$$

$$S_{CO_2} = \frac{Y_{CO_2}}{\chi_{CH_3OH}} \qquad\qquad 2.8$$
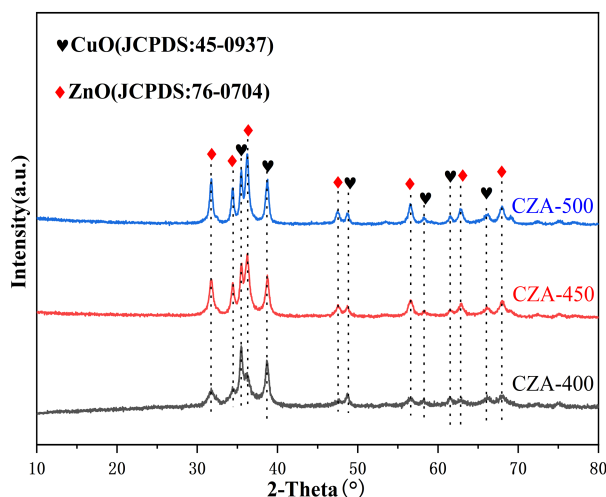
3. Results and discussion

3.1 XRD

Fig. 1 XRD patterns of CZA-X catalysts

X-ray diffractograms of CZA-X are shown in Fig. 1. X-ray diffraction (XRD) analysis showed that the main phases present in CZA-X were copper oxide (CuO) with monoclinic crystal phase (JCPDS No. 45-0973) and zinc oxide (ZnO) with hexagonal crystal phase (JCPDS No. 76-0704), thereby confirming the decomposition of precursor into CuO and ZnO during catalyst calcination. Furthermore, it was noticeable that the decrease in the widths of diffraction peaks was observed for these three catalyst samples with the increasing calcination temperature from 400 to 500℃, which should be closely associated with the formation of the larger crystallite size accompanied with the small specific surface area, as further confirmed in Table. 1. Besides, the diffraction patterns of all samples showed that no Al_2O_3 phases were detected, this was probably due to the relative lower composition and high dispersion of aluminium or the detection limit for XRD measurement, this is consistent with Yong-jun Liu result [11].
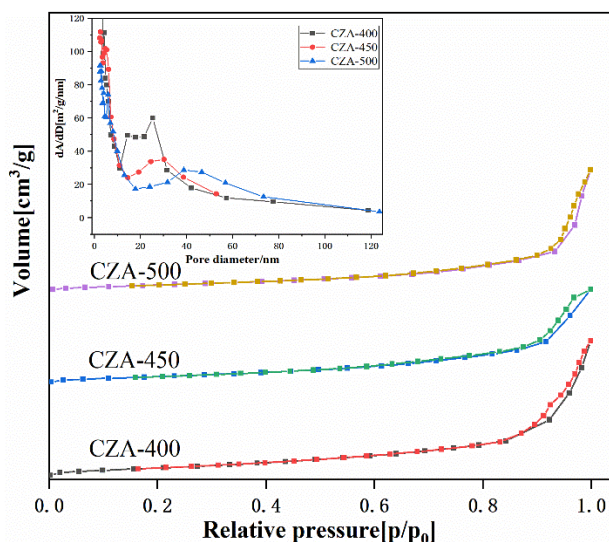
3.2 BET

Fig. 2 N₂ adsorption-desorption and pore diameter distribution isotherms of the CZA-X catalysts

Table. 1 illustrated the physical characteristics of samples which was measured by BET and N₂O titration method. One could see that, as the calcination temperature increased, the specific surface area of catalyst, the

dispersion of Cu (D_{Cu} %) and exposed Cu surface area (S_{Cu} m²/g) decreased significantly, while its average pore size increased, when the calcination temperature was 500°C, the surface area of the material and the dispersion of Cu minimum 32.81 m²/g and 7.26%, respectively, which could be attributed formation of the larger crystallite size at higher temperatures. The result is consistent with the CuO/CeO_2 catalyst prepared at different calcination temperature by solvent-free method [12]. Fig. 2 showed the N_2 adsorption-desorption isotherms of the catalysts. Regardless of the calcination temperature used, each of the CZA-X showed a type IV isotherm, together with a H_3 type hysteresis loop of varied size with a maximum of pore size distribution at 20-40 nm mesoporous materials [13, 14]. Furthermore, mesoporous materials with smaller pore size showed better candidates for hydrogen storage [15]. It was also found that BET surface area decreased, whereas the average pore diameter increased after the increasing the calcination temperature, which was common rule in our catalysts, there by illustrate the crystal particles grow up during reaction and main pore size was large.

3.3 SEM

The scanning electron microscopy (SEM) images of all the samples were shown in Fig. 3. It was showing that hierarchically porous CZA-X microspheres, which assembled with nanosheet. Fig. 3 (a_2, b_2, c_2) shown the locally amplified SEM image of CZA-X to investigate the structural details of samples which CZA-400 microspheres without structural collapsed. Moreover, CZA-450 was to be found the size of nanosheet greater than CZA-400, due to with increasing calcination temperature facilitated Ostwald ripening, that induced the nanosheet growth. In addition, uniform and monodisperse microspheres structural local collapse can be clearly found in the CZA-500 image (Fig. 3 c_2), which might be due to the higher calcination temperature [16]. This result was coincident with BET results in Table. 1.
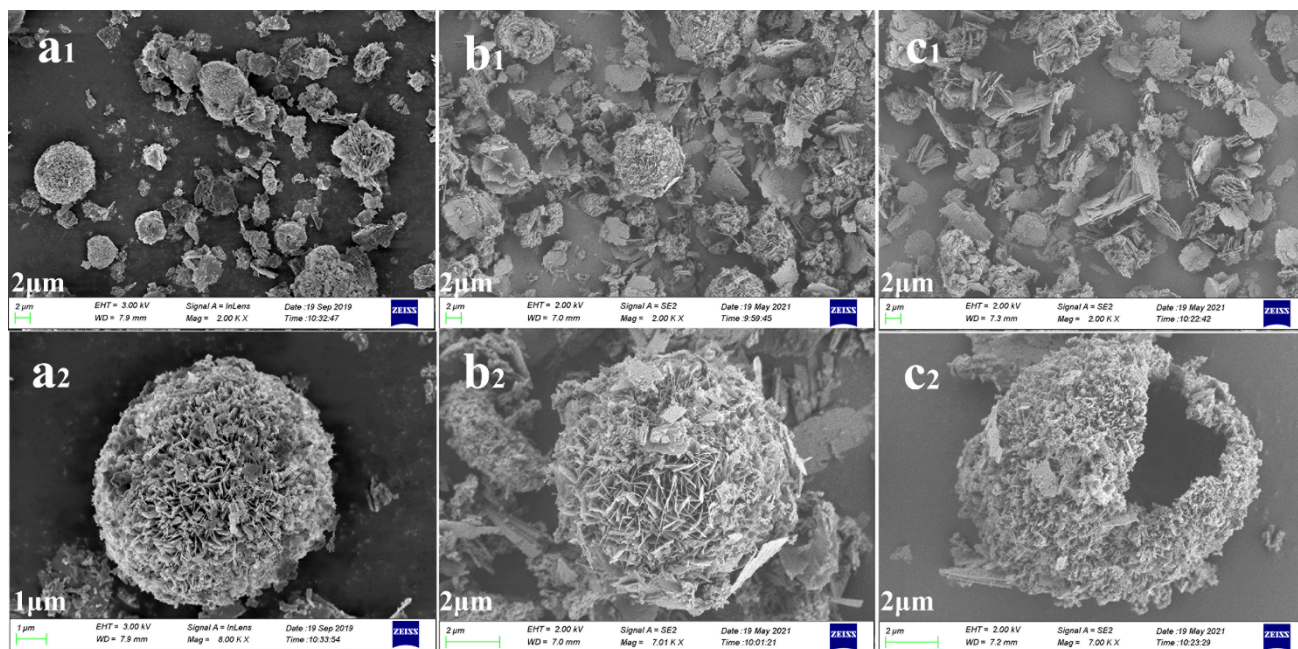

Fig. 3 SEM images of CZA-X. a : CZA-400; b : CZA-450; c : CZA-500

Table 1 Physical characteristics of the prepared samples

Catalysts	$S_{BET}(m^2/g)$	Total pore volume (cm³/g)	Average pore size (nm)	Cu dispersion (%)	S_{Cu} (m²/g)
CZA-400	50.42	0.276	10.95	18.16	122.85
CZA-450	40.52	0.193	9.50	11.35	76.80
CZA-500	32.81	0.245	14.94	7.26	49.08

3.4 TG

Calcination of precursor samples was simulated by TG (Thermogravimetric Analysis) experiment, the precursors of Cu and Zn were prepared by the same method for comparison, with the results shown in Fig. 4 (a). It can be seen that the decomposition of precursor Zn was completed by one step and change was not obvious of precursor Cu, while the Cu/Zn/Al catalyst precursors were decomposed gradually with increasing temperature. In the TG profile of sample Cu/Zn/Al, the weightless of 200 to 400°C were main ascribed to the decomposition of precursor Zn.
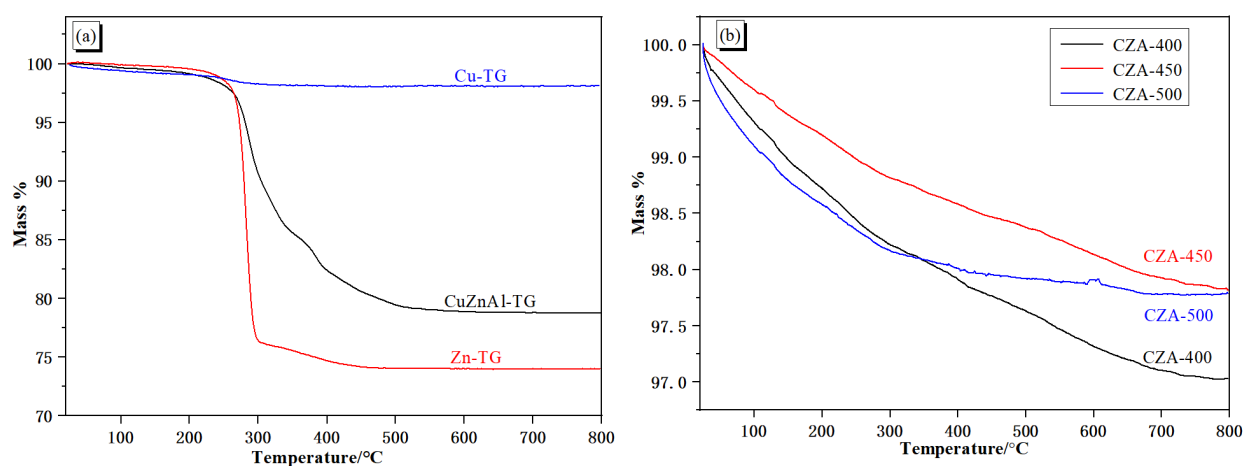

Fig. 4 Thermogravimetric analysis (TG) of (a): Cu precursor, Zn precursor, CZA precursor, (b) CZA-X

In addition, the thermal stabilities of CZA-400, CZA-450 and CZA-500 evaluated by TG were represented in Figure. 4 (b), with a total mass loss of 2.22%, 2.18%, and 3.00%, respectively. The result exhibited CZA-400 lower stability and corroborates the detected by BET and SEM.
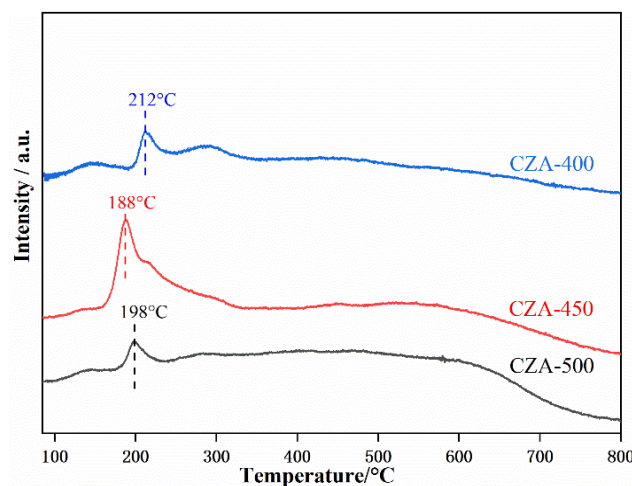
3.5 CO₂-TPD

Fig. 5 CO$_2$-TPD curves by CZA-X samples

The CO$_2$ desorption curves (CO$_2$-TPD) of the CZA-X samples displayed in Fig. 5. As seen from Fig. 5, the desorption peaks appeared in two temperature ranges of 100-200°C and 200-500°C, which were attributed to weak and strong basic sites on the surface of the catalysts, respectively [17]. Moreover, it can be found that the CZA-450 possessed relatively weaker basic sites than strong basic sites, and its CO$_2$ main desorption temperature (188°C) lower than CZA-400 and CZA-500, while the desorption peak areas of CZA-500 was smaller than others, it could be due to the specific surface area of CZA-500 and the larger crystallite size.
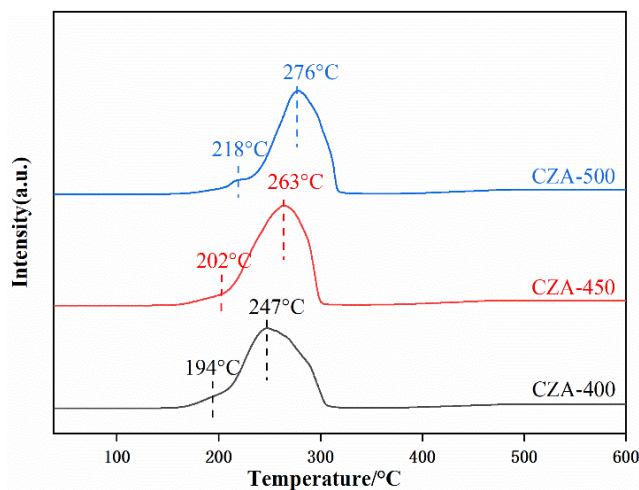
3.6 H$_2$-TPR

Fig. 6 H$_2$-TPR profiles of CZA-X catalysts

To investigate the reduction behaviour of the CZA-X catalysts, TPR experiments were carried out. As observed in Fig. 6, the reduction profiles of the CZA-X samples demonstrated two reduction peak, with reduction temperatures in range of 100 to 350°C, the reduction peak at around 200°C was assigned to the reduction of highly disperse CuO to Cu^0, and the peak at around 260°C was attributed to the reduction of bulk-like CuO to Cu^0 [18, 19]. It was apparent that the dominated Cu species were CuO in these samples, which is consistent with XRD. Additionally, the reduction temperature of Cu species is closely related to its dispersion state over support, and

the Cu species with higher dispersion are more easily reduced [20]. Meanwhile, it was clearly seen that the main peaks shifted to higher temperature for CZA-450, CZA-500, the amount of highly disperse CuO decreased and moved to higher temperatures, demonstrating that CuO could be reduced more difficulty to Cu^0. The S_{Cu} and D_{Cu} reducing (Table. 1) with the increasing of the calcination temperatures, which suggested that the higher calcination temperature caused a strong interaction among Cu and Zn or Al oxides [21]. Thus, it can be founded that the forms of CuO were obviously distinct at different calcination temperature for CZA samples.
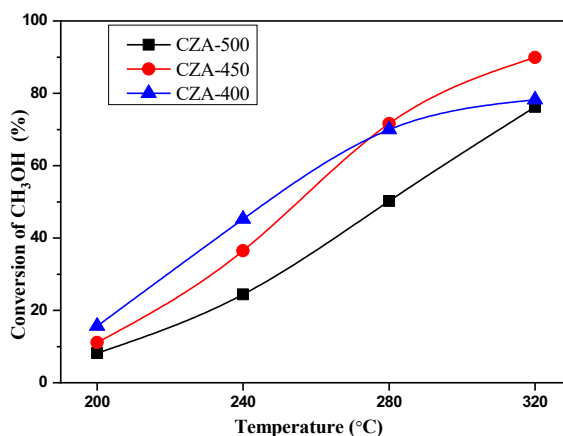
3.7 Catalyst activity

Fig. 7 Methanol conversions related to reaction temperature

The catalytic performance of catalysts for steam reforming of methanol (SRM) was given in Fig. 7. As seen from Fig. 7, For the CZA catalysts, the CH_3OH conversion increased with increasing temperature and the highest conversion was obtained at 320°C, which is consistent with results reported in the literature [22, 23]. In the case of CZA-500, the lowest catalytic performance was obtained at 200-320°C compared to the CZA-400 and CZA-450 catalysts, which may be due to the larger particle size, smaller surface area and lower dispersion of Cu The CZA-400 catalyst had higher conversion under 280°C than other samples, which could be due to its higher dispersion of Cu and larger surface area. While CZA-450 showed excellent CH_3OH conversion performance at higher temperature (320°C), it can be attributed to its better thermal stability.
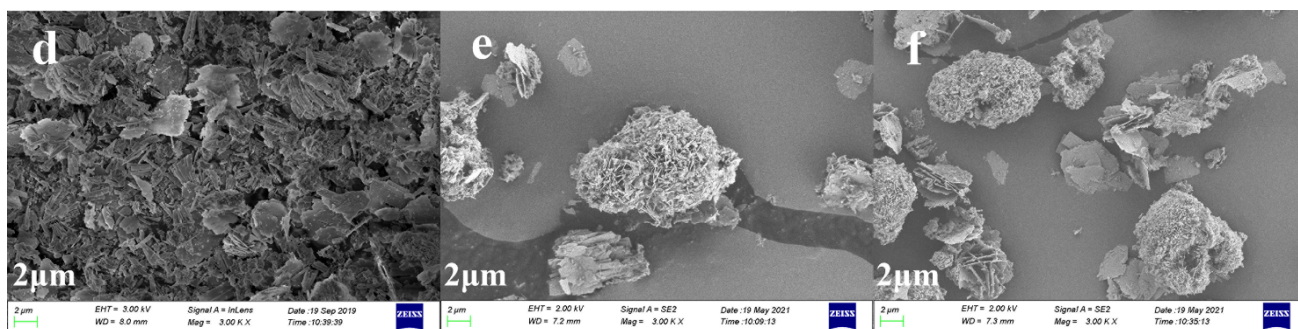

Fig. 8 SEM images of recovered samples CZA-400(d); CZA-450(e); CZA-500(d)

The BET and SEM experiments were carried out for recovered samples to explore the influence on the structure of catalyst in the reaction process, as shown in Table. 2 and Fig. 8. Compared to the fresh samples, the specific surface area of recovered CZA-500 and CZA-450 samples almost unchanged and its SEM images also

had no significant differences compared to fresh samples, respectively, which can demonstrate its higher stability. Notably, the specific surface area of CZA-500 is small and structure local collapses. For CZA-400, not only its surface area significant decreased, but also the microspheres collapsed due to its low stability. In the present work, the differences in calcination temperature resulted in differences interactions between the active metals with Zn and Al oxide. As such, a significant difference in CH_3OH conversion and CO_2/CO selectivity were observed.

Table. 2 BET of recovered catalysts

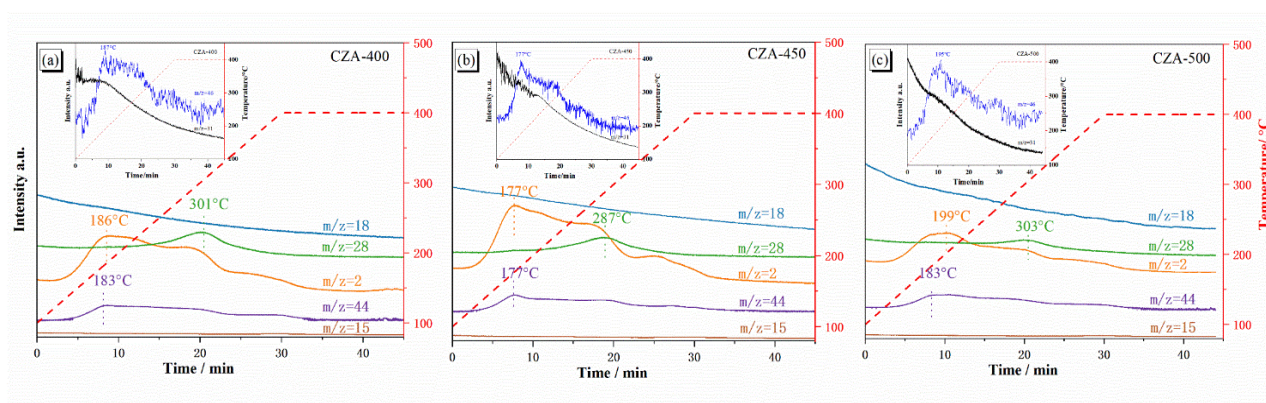| Catalysts	$S_{BET}(m^2/g)$	Total pore volume (cm^3/g)	Average pore size（nm）
CZA-400(Recovery)	36.83	0.326	17.71
CZA-450(Recovery)	39.99	0.289	14.43
CZA-500(Recovery)	32.13	0.328	20.42

3.8 CH₃OH-TPD

Fig. 9 CH₃OH-TPD profiles of different catalysts

To further understand the decomposition mechanism of CH_3OH on CZA-X catalysts, CH_3OH-TPD were conducted, and the results of which are shown in Fig. 9. For the CZA-X samples, there was an obvious H_2 (m/z=2) and CO_2 (m/z=44) formation, except for H_2 and CO_2, other products such as H_2O (m/z = 18), CO (m/z = 28), CH_4 (m/z = 15), CH_3COOH (m/z = 46), and CH_3OH (m/z = 31) were also monitored [24]. The H_2 formation peak shifts to lower temperature, which indicate that the samples are favourable to the decomposition of CH_3OH [25]. It can be seen that the H_2 (m/z = 2) formation peaks of CZA-400, CZA-450 and CZA-500 were located at 186, 177 and 199°C, respectively, in which the temperature of CZA-450 is the lowest, indicating that it is easier to activate and dissociate methanol, while for the CZA-500 the products peak temperatures were higher than others, which corresponds to the lowest catalytic activity of CZA-500 as shown in Fig. 7. It was worth that CH_3COOH (m/z=46) was detected with the formation of H_2, demonstrating that CH_3OH was adsorbed and then transformed into CH_3COOH (m/z=46), finally CH_3COOH (m/z=46) were decomposed into products. In addition, no methanol desorption peaks were detected, which assigned to the limit of MS instruments and the high temperature (100°C) of methanol adsorption. Notably, there was an obvious CO (m/z=28) peaks around 300 °C, which may be attributed to products(H_2+CO_2) could be react in high temperature, and CO_2+H_2-TPSR were performed.
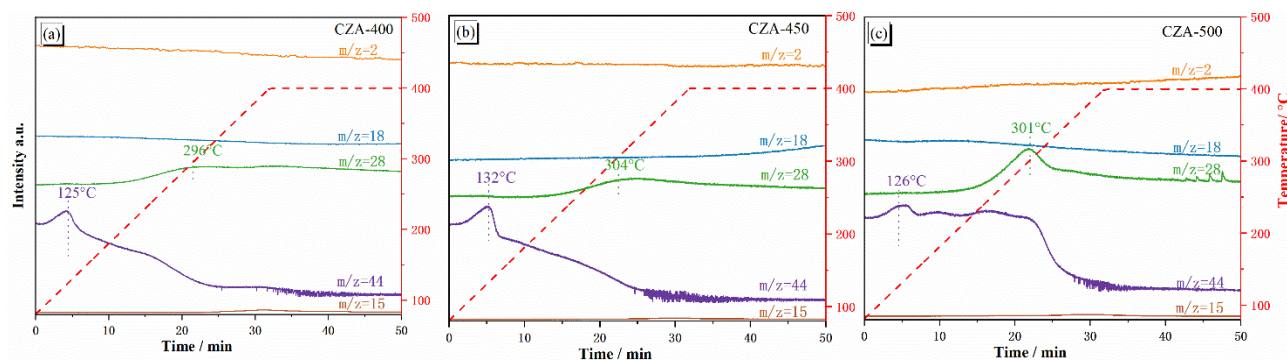
3.9 CO₂+H₂-TPSR

Fig. 10 CO_2+H_2O-TPSR profiles

For exploring the reverse water gas shift reaction (RWGS) performance, the RWGS reaction (CO_2 + H_2 → CO + H_2O) was carried out by CO_2+H_2-TPSR, which the result being showing in Fig. 9. Exhaust compositions such as CO (m/z = 28), H_2(m/z=2), CO_2 (m/z=44), H_2O (m/z=18) and CH_4 (m/z=15), were monitored. As seen from Fig. 10, the CO_2 (m/z=44) desorption occurs at 130℃ over all the catalysts, which related to the CO_2-TPD experiment in Fig. 5, which was attributed to the desorption of CO_2 at weak basic sites. In addition, the peak of CO appeared at about 300℃, the RWGS reaction is endothermic, indicating that thermodynamically favoured by higher temperatures [26-28] which may be related to the poor activity of CZA-400 at high temperature due to its high CO selectivity at high temperature. Notably, nearly no obvious H_2 consumed signal for all samples, which could be assigned to the consumption of higher concentration of H_2 (10% H_2/Ar).

Conclusions

In summary, the different calcination temperature of Cu/Zn/Al catalysts had an obvious influence on the physical characteristics and catalytic performance of the methanol steam reforming. The higher calcination temperature of Cu/Zn/Al catalyst not only increased the stability, but also enhanced stronger interaction among Cu and Zn or Al oxides, while the structure of Cu/Zn/Al catalyst destroyed when on the high temperature (500℃) calcination, which caused the poor performance. Raising temperature favoured the decomposition of methanol in CZA-X catalyst. The catalytic performance of CZA-400 was better than CZA-450 when reaction temperature under 280℃. However, the conversion of CH_3OH reached above 90% over CZA-450 catalyst when the reaction temperature was 320℃, which showed excellent performance than others. BET and SEM studies provided that the CZA-450 had higher stability than CZA-400. Meanwhile, CH_3OH-TPD showed that CZA-450 more trend to decomposition of CH_3OH.

Acknowledgements

References

[1]. Shen Y, Zhan Y, Li S, Ning F, Du Y, Huang Y, He T, Zhou X (2017) Chemical Science 8:7498-7504.

[2]. Qi T, Yang Y, Wu Y, Wang J, Li P, Yu J (2018) Chemical Engineering and Processing - Process Intensification 127:72-82.

[3]. Díaz-Pérez MA, Moya J, Serrano-Ruiz JC, Faria J (2018) Industrial & Engineering Chemistry Research 57:15268-15279.

[4]. Nowicka E, Althahban SM, Luo Y, Kriegel R, Shaw G, Morgan DJ, He Q, Watanabe M, Armbrüster M, Kiely CJ, Hutchings GJ (2018) Catalysis Science & Technology 8:5848-5857.

[5]. Tang C-W, Chen Y-J, Yeh C-T, Wu R-C, Wang C-C, Wang C-B (2021) International Journal of Hydrogen Energy 46:80-88.

[6]. Qiao W, Yang S, Zhang L, Tian Y, Wang H, Zhang C, Gao Z (2021) International Journal of Energy Research 45:12773-12783.

[7]. Kubacka A, Fernández-García M, Martínez-Arias A (2016) Applied Catalysis A: General 518:2-17.

[8]. Ma H, Zhou M, Ying W, Fang D (2016) International Journal of Hydrogen Energy 41:16932-16943.

[9]. Palo DR, Dagle RA, Holladay JD (2007) Chemical Reviews 107:3992-4021.

[10]. Lei H, Hou Z, Xie J (2016) Fuel 164:191-198.

[11]. Liu Y-J, Deng X, Han P-D, Huang W (2017) International Journal of Hydrogen Energy 42:24757-24766.

[12]. Wang J, Zhong L, Lu J, Chen R, Lei Y, Chen K, Han C, He S, Wan G, Luo Y (2017) Molecular Catalysis 443:241-252.

[13]. Liu Y-J, Deng X, Jia L, Huang W (2018) Physical Chemistry Chemical Physics 20:18790-18799.

[14]. Han F, Liu H, Cheng W, Xu Q (2020) RSC Advances 10:33620-33627.

[15]. Liu Y, Lu J, Yang J, Zhang Y, Wang J, Li C, Xia L (2018) Materials Letters 214:91-94.

[16]. Cheng S-Y, Kou J-W, Gao Z-H, Huang W (2018) Applied Catalysis A: General 556:113-120.

[17]. Gao Z, Liu Y, Li L, Li S, Huang W (2017) Energy Sources, Part A: Recovery, Utilization, and Environmental Effects 1-7.

[18]. Zuo Z-J, Wang L, Liu Y-J, Huang W (2013) Catalysis Communications 34:69-72.

[19]. Gao P, Li F, Xiao F, Zhao N, Sun N, Wei W, Zhong L, Sun Y (2012) Catalysis Science & Technology 2:1447-1454.

[20]. Zhang G, Zhao D, Yan J, Jia D, Zheng H, Mi J, Li Z (2019) Applied Catalysis A: General 579:18-29.

[21]. Deng X, Liu Y-J, Huang W (2018) Journal of Energy Chemistry 27:319-325.

[22]. Sarafraz MM, Safaei MR, Goodarzi M, Arjomandi M (2019) International Journal of Hydrogen Energy 44:19628-19639.

[23]. Cai F, Lu P, Ibrahim JJ, Fu Y, Zhang J, Sun Y (2019) International Journal of Hydrogen Energy 44:11717-11733.

[24]. Araiza DG, Gómez-Cortés A, Díaz G (2017) Catalysis Today 282:185-194.

[25]. Zhang L, Meng M, Wang X, Zhou S, Yang L, Zhang T, Zheng L, Zhang J, Hu T (2014) Journal of Power Sources 268:331-340.

[26]. Pastor-Pérez L, Baibars F, Le Sache E, Arellano-García H, Gu S, Reina TR (2017) Journal of CO2 Utilization 21:423-428.

[27]. Parra AAM, Asmanoglo C, Agar DW (2017) Chemical Engineering & Technology 40:915-926.

[28]. Zhang X, Zhu X, Lin L, Yao S, Zhang M, Liu X, Wang X, Li Y-W, Shi C, Ma D (2017) ACS Catalysis 7:912-918.